FULL PAPER

PPS www.rsc.org/pps

Photoelectrochemical measurements of a heterosupramolecular system under visible light irradiation

Gregory J. Wilson and Geoffrey D. Will
Inorganic Materials Research Program, Queensland University of Technology, Brisbane, Queensland, Australia. E-mail: g.will@qut.edu.au; Fax: +61 07 3864 1807; Tel: +61 07 3864 2297

Received 17th March 2005, Accepted 15th June 2005
First published as an Advance Article on the web 4th July 2005

A photochemical system utilising a modular approach characterised through interpretation of photoelectrochemical measurements is discussed. A photoanode was prepared by the chemisorption of a photosensitiser, *cis-bis*-(2,2′-bipyridine)-(4,4′-bis-(methyl)phosphonato-2,2′-bipyridine)ruthenium(II) dichloride ($RuL_2L'^{2+}$), to a mixed nanoporous nanocrystalline RuO_2:TiO_2 thin film, calcined on a fluorine doped SnO_2 conducting glass substrate. Similarly, an electron relay molecule, 1-ethyl-1′-(2-phosphonoethyl)-4,4′-bipyridinium dichloride (EVP), was covalently bound to a platinum electroplated nanoporous nanocrystalline TiO_2 thin film, and the electrodes connected in a photoelectrocatalytic cell (PCC). Irradiation with $\lambda > 420$ nm gave a measurable photocurrent. Interpretation of the photocurrents obtained from this assembly provides a means for understanding photochemical reactions under low light intensities. Optimised conditions of the electrolyte solution were determined to be pH = 5 and illumination yielded $\eta = 0.0036\%$ with an apparent quantum yield (AQY) = 1.6%.

Introduction

Photocatalysis using n-type semiconductors is well-established. TiO_2 is often utilised in such systems since it is a robust metal oxide with excellent photocatalytic properties.[1] Electron-hole pair generation affords these attractive properties through charge trapping derived from defect sites of the crystal lattice surface.[2] The crystalline structure of TiO_2 lends itself to these properties with the rutile phase common for this purpose. Research in this field was initiated by the report of Fujishima and Honda.[3] They utilised a single crystal of rutile TiO_2 to achieve photoassisted cleavage of water through bandgap excitation with UV light. Their study involved the use of a TiO_2 photoanode and a platinum cathode irradiated with UV light and assisted by an applied bias (>0.25 V). TiO_2, due to its photocatalytic properties, is widely studied in relation to the production of hydrogen[4–6] and/or the photodegradation of organic/biological waste in aqueous environments.[7–10]

Hydrogen generation is an achievable goal for solar energy conversion and storage with TiO_2 a cheap and affordable medium for its production. However TiO_2 is not an efficient photocatalyst (with a bandgap of 3.2 eV). Electron-hole formation necessitates a larger overpotential than is thermodynamically required to achieve water photolysis [eqn. (1) and (2)]:

$$2H_2O_{(l)} \rightarrow O_{2(g)} + 4H^+_{(aq)} + 4e^- \; E^\circ = +0.82 \text{ V } \S \qquad (1)$$

$$2H_2O_{(l)} + 2e^- \rightarrow H_{2(g)} + 2OH^-_{(aq)}, \; E^\circ = -0.41 \text{ V } \S \qquad (2)$$

§ *versus* SHE at pH = 7.

The Gibbs free energy change for the overall photolysis reaction is 237.2 kJ mol^{-1}. Thus, the reaction is non-spontaneous and requires an input of energy that corresponds to 2.46 eV per molecule of water to drive the reaction to completion. This equates to 1.23 eV per electron or a photon with a wavelength of $\lambda < 1008$ nm. Hence the photolysis of water can be theoretically and thermodynamically met by a photon from the visible region of the solar spectrum.

An alternative to solid-state photocatalysis is the solution based photochemical production of hydrogen.[11–13] This approach involves the use of molecular species in solution, acting as intermediates, to undertake specific functions in the photochemical process. Thus this can effectively overcome the inability of water to absorb appreciable amounts of energy in the visible region of the electromagnetic spectrum. Desirable functions of intermediates include: visible light absorption; conversion of excitation energy to redox energy; and the transfer of excited electrons to and from water to evolve H_2 and O_2.

Many model photochemical systems have been devised, reported and reviewed.[14] In particular Moradpour *et al.*[15] and Kalyanasundaram *et al.*[16] similarly reported the classical and simplistic $Ru(bpy)_3^{2+}$ system for the photoassisted degradation of water. This system utilises a photosensitiser (PS), an electron shuttle molecule and a microheterogeneous catalyst for the photolysis of water using photons of visible light. The system depends on the reduction potentials of the relevant species in solution and the chance collisions of all components.

Further, the reports by Kalyanasundaram and co-workers[16,17] and Grätzel and co-workers[18,19] combined the broad spectral response from a PS with that of composite photocatalytic systems. The use of TiO_2 with H_2 and O_2 specific catalysts, Pt and RuO_2 respectively, mediated photoinduced water splitting. These systems describe composite particles imitating a micro-photoelectrochemical (PEC) cell with RuO_2 as the anode and Pt as the cathode. The results of these early reports have been difficult for other laboratories to reproduce.[20,21] Despite this the conclusion that the overpotential required for the direct photolysis of water, under bandgap excitation, is significantly reduced in the presence of mixed catalytic particles has been established.[22–27] Indeed, a recent study by Currao *et al.* identified stoichiometric quantities of H_2 and O_2, and hence water splitting, by a self-sensitised PEC cell in the presence of noble metals.[28]

In this study we present a modular approach to the assembly of a photochemical system, a heterosupramolecular system.[29–31] Our current investigation presents evidence of photochemical reactions occurring in aqueous media through analysis of photochemical measurements. Further optimisation of the system under the current configuration may provide an effective medium for cyclic water splitting. The concept of this system is represented in Scheme 1.

DOI: 10.1039/b503873a

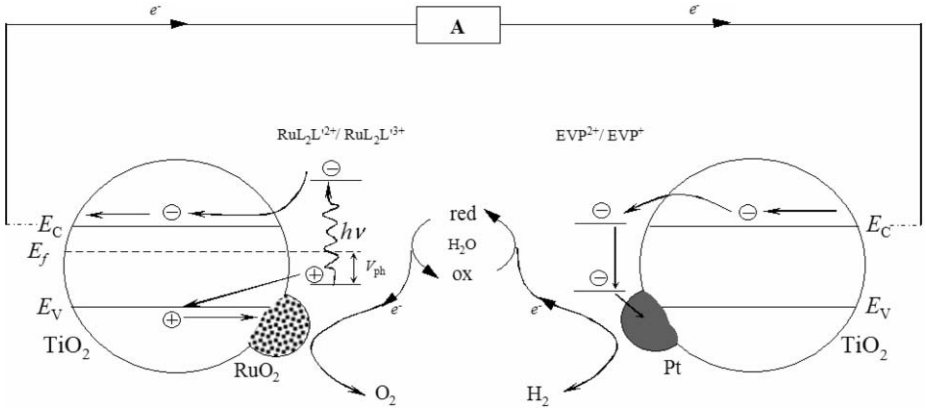

Scheme 1 Schematic representation of the heterosupramolecular approach to simultaneous O_2 and H_2 production.

Experimental

Materials

All reagents and solutions were prepared from analytical grade reagents (AR) used as received from Sigma-Aldrich. The ligand 4,4′-bis-diethyl(methyl)phosphonate-2,2′-bipyridine (dempbpy) was prepared according to a procedure by Gillaizeau-Gauthier *et al.*[32] with a yield of 70%. *Cis*-bis-(2,2′-bipyridine) dichlororuthenium(II) hydrate ($RuL_2Cl_2^0$) was prepared and purified as described by Sullivan *et al.*[33] The characterisation of all ligand and molecular components was recorded as ^1H, ^{13}C or ^{31}P NMR spectra on a Bruker NMR spectrometer at 400, 100 and 162 MHz respectively. ^1H chemical shifts [δ (ppm)] are referenced to the residual solvent signal; ^{13}C δ are referenced externally to acetone and ^{31}P δ are referenced externally to 85% H_3PO_4. Absorption spectra were obtained using the Varian Cary 50 UV-Visible spectrometer and emission spectra obtained on the Varian Eclipse UV-Fluorescence Spectrometer in the indicated solvents. Conducting glass substrates were TEC15/3 fluorine doped tin oxide from Libby Owens Ford (LOF) ~1.6 mm thick with a nominal resistivity of 15 Ω cm^{-2} abbreviated as F:SnO_2. Ultrahigh purity (UHP) deionised water (18.2 MΩ) was treated by Millipore filtration prior to distillation over $KMnO_4$ to remove ionic and organic contaminants. UHP water so treated was used for all preparations involved in this study. Solution pH was determined using a pH 330i meter and a Sentix 41 pH electrode (WTW, Weilheim) using a conventional two-point calibration. This gave UHP H_2O (pH = 6.2) and 0.5 M Li_2SO_4 (pH = 5.7).

Preparation of catalytic RuO_2 nanocrystals

A procedure adapted from Ardizzone *et al.*[34] was followed for the preparation of crystalline RuO_2. Briefly, $RuCl_3$ (415 mg) was dissolved in 20% HCl, evaporated at 80 °C and redissolved in isopropanol prior to decomposition in a muffle furnace at 350 °C for 90 min. The metallic crystalline material was mechanically treated before returning to the furnace for a further 6 h at 450 °C. The prepared crystalline RuO_2 was washed with high, low and pH 7 deionised water and filtered to remove all residual $RuCl_3$. Approximately 200 mg (75%) of RuO_2 was isolated.

Preparation of nanoporous nanocrystalline TiO_2 films

Colloidal TiO_2 solution was prepared by the hydrolysis of titanium isopropoxide following an experimental procedure adapted from O'Regan *et al.*[35]

Nanoporous TiO_2 and mixed metal oxide films were prepared by spreading a small quantity of the concentrated dispersion with a glass rod on a F:SnO_2 substrate.[36] Resulting films were air dried for 45 min prior to sintering in a muffle furnace at 450 °C in air for 12 h. The films, denoted TiO_2 and RuO_2:TiO_2 respectively, were stored in a darkened vacuum desiccator until required.

Electrodeposition of platinum

In a three-electrode system, the working electrode was a F:SnO_2 substrate or modified film, a platinum wire counter and referenced against a saturated calomel electrode (SCE). The electrodes were immersed in a hexachloroplatinic acid solution (2.1×10^{-3} M) degassed for 10 min with high purity N_2 prior to the electroplating sequence. A potential sweep from 0 to −0.8 V with deposition for 30 s at −0.8V over 5 cycles gave a darkened platinised surface. Potentiostatic control was provided by the EG & G Princeton Applied Research model 272A potentiostat/galvanostat. Following the procedure, the electrode surface was rinsed with deionised water and stored in a darkened vacuum desiccator until required.

Preparation of molecular components

The electron donor molecule, *cis*-bis-(2,2′-bipyridine)-(4,4′-bis-(methyl)phosphonato-2,2′-bipyridine) ruthenium(II) dichloride ($RuL_2L'^{2+}$) was prepared in a procedure analogous to Gillaizeau-Gauthier *et al.*[32] This gave $RuL_2L'^{2+}$ as a dark orange hygroscopic solid (yield 117 mg, 89%). ^1H NMR (400 MHz, D_2O, δ): 2.84 (d, $^2J_{PH} = 20$ Hz, 4H) CH_2P; 7.04 (m, $J = 5.1$ Hz, 2H) H_{5a}, $H_{5a'}$; 7.16 (m, $J = 5.4$ Hz, 4H) H_5, $H_{5'}$; 7.28 (d, $J = 5.1$ Hz, 1H) $H_{6a'}$; 7.41 (m, $J = 5.4$ Hz, 2H) $H_{4'}$; 7.54 (m, $J = 5.1$ Hz, 1H) H_{6a}; 7.64 (d, $J = 5.4$ Hz, 2H) $H_{6'}$; 7.77 (d, $J = 5.4$ Hz, 2H) H_6; 7.84 (m, $J = 8.0$ Hz, 2H) H_4; 8.22 (s, 2H) H_{3a}; 8.33 (m, $J = 8.0$ Hz, 4H) H_3. ^{31}P NMR (162 MHz, D_2O, δ): 15.19, $CH_2PO_3H_2$. Calculated for $RuC_{32}H_{30}N_6O_6Cl_2P_2{\cdot}9H_2O$: C, 38.80; H, 4.88; N, 8.48; Found C, 38.33; H, 4.12; N, 7.99. Absorption (MeOH): $\lambda_{max} = 455$ nm ($\varepsilon_{455} = 13.1 \times 10^3$ mol dm^{-3} cm^{-1}). Emission (MeOH): $\lambda_{max} =$ 612 nm.

The electron relay molecule, 1-ethyl-1′-(2-phosphonoethyl)-4,4′-bipyridinium dichloride (EVP), was prepared according to the procedure described by Cinnsealach *et al.*[37] In a two step procedure EVP was isolated as a fine white powder (yield 4.48 g, 80%). ^1H NMR (400 MHz, DMSO-d_6, δ): 1.58 (t, $J = 7.28$ Hz, 3H) CH_3; 2.45 (dt, $J = 7.95$ Hz, 2H) CH_2P; 4.73 (q, $J = 7.28$ Hz, 2H) $^+NCH_2CH_3$; 4.90 (dt, $J = 12.94$ Hz, $J = 7.65$ Hz, 2H)$^+NCH_2CH_2P$; 8.84 (dd, $J = 4.60$ Hz, 4.77 Hz, 4H) $H_{3,5}$, $H_{3b,5b}$; 9.46 (m, $J = 6.98$ Hz, 6.81 Hz, 4H) $H_{2,6}$, $H_{2b,6b}$. ^{13}C NMR (100 MHz, D_2O, δ): 16.21 CH_3; 29.83 (d, $^1J_{PC} = 132.98$ Hz) CH_2P; 58.16 CH_2CH_2; 58.31 CH_2; 127.58 C_{3b}, C_{5b}; 127.65 C_3, C_5; 145.85 C_{2b}, C_{6b}; 146.31 C_2, C_6; 150.55 C_{4b}; 151.11 C_4. ^{31}P NMR (162 MHz, D_2O, δ): 19.06.

The structures of $RuL_2L'^{2+}$ and EVP are depicted in Scheme 2.

Chemisorption of molecular components to thin film electrodes

To achieve covalent binding of the surface sensitisers, films were heated to 120 °C for 20 min to remove adsorbed water, before cooling to approximately 80 °C. Films were then immersed immediately in a solution of the molecular component (typically

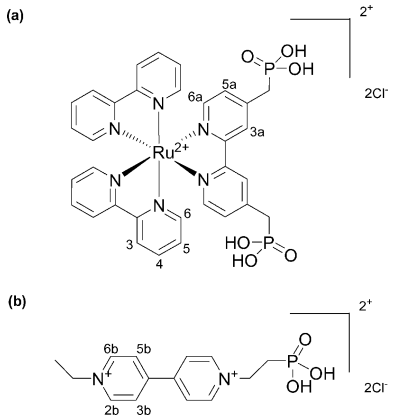

Scheme 2 Structure of (a) the electron donor ($RuL_2L'^{2+}$) and (b) electron acceptor (EVP) molecules as utilised in the photochemical system. Numbering system for NMR resonance assignment as indicated.

3.27×10^{-3} M). Chemisorption was achieved after 10 h, the films were removed and rinsed in deionised water. The films were stored in a darkened vacuum desiccator until required. The assembly of the electrodes for individual experiments are detailed in Table 1.

Photoelectrochemical measurements

Samples were analysed in a photoelectrocatalytic cell (PCC) with an exposed electrode surface area (2.30 cm^2) in contact with the electrolyte solution. The cell volume was 100 cm^3 with a spatial distance of 2.8 cm between the electrodes. Measurements were obtained in UHP water that contained Li_2SO_4 (0.5 M) as electrolyte at pH 5.7. The cell was illuminated using a high intensity white light LED for visible irradiation in the range 400–750 nm. The purpose built LED source consisted of a cluster of 7 × 5 mm round water-clear LED lenses, collimated to a focal point. The LED source was regulated *via* a ten position digital resistor, with measurements obtained at 3.81 mW cm^{-2}.

Table 1 Scheme for nomenclature and assembly of electrodes. A '/' indicates subsequent treatment, while ':' indicates a composite material

Electrode	Electrode assembly
I	$TiO_2/F:SnO_2$
II	$RuO_2:TiO_2/F:SnO_2$
III	$Pt/TiO_2/F:SnO_2$
IV	$RuL_2L'^{2+}/TiO_2/F:SnO_2$
V	$EVP/TiO_2/F:SnO_2$
VI	$EVP/Pt/TiO_2/F:SnO_2$
VII	$RuL_2L'^{2+}/RuO_2:TiO_2/F:SnO_2$

For increased light intensity the illumination source was a 150 W Xe arc lamp (Oriel) passed through a 90° IR mirror. A Schott KG4 (Oriel #51942) was used to emulate AM1.5 conditions and limited to $\lambda > 420$ nm with a cut-off filter (Oriel # 66420). The beam was focused at the surface of the cell (12.0 mW cm^{-2}).

Data was recorded using the PT-104 4-channel data logger (Pico Technology Limited, St Neots, Cambridgeshire, UK) interfaced to an IBM compatible PC. Data was logged (PicoLog for Windows, release 5.09.4) at a rate of one sample per second, averaged over the collection period, with a resolution of $\pm 5.2 \times 10^{-5}$ μA. Measurements were collected using a differential 3 wire input with ground across a 3 kΩ resistor. Samples were placed in an optically dark box for several minutes prior to illumination. Light intensities were determined with a Power Max 5100 laser power meter (Molectron Detector Inc., Portland, OR).

Results and discussion

Investigation of the photochemical assembly using the LED source

Electrochemical assemblies for individual experiments are summarised in Table 2. For each assembly the limiting current (j_{lim}) under steady-state oxidation after 60 seconds of illumination is detailed.

In our preliminary report we proposed conceptually the use of a photochemical system immobilised on a semiconducting substrate.[31] The following data is for photocurrents obtained, using this photochemical system, in an aqueous medium.

Experiments 1–4 utilise a TiO_2 thin film as a photoanode. TiO_2 (band gap = 3.2 eV for the anatase crystalline phase) requires a photon of $\lambda < 387$ nm for surface activation, which was unobtainable under the current experimental conditions. The negligible photocurrents obtained provide evidence of the inability of TiO_2 to effectively photooxidise water under white light irradiation.

Surface modification of the TiO_2 electrode by the adsorption of $RuL_2L'^{2+}$ as a PS provides a spectral response that coincides with that of the illumination source. The peak absorption band for $RuL_2L'^{2+}$ was centred at 455 nm which corresponds with the peak emission of the white light LED cluster of 462 nm. The adsorption of $RuL_2L'^{2+}$ to the surface affords several advantages: (i) improved spectral overlap in the visible region; (ii) electron-charge separation isolated from the semiconductor; and (iii) intimate contact of the PS with TiO_2 for direct electron injection to the conduction band (CB). The inclusion of $RuL_2L'^{2+}$ alone to the cell assembly leads to an increase in the observed photocurrent. Therefore the inclusion of the PS (exp. 5) provides efficient charge separation that subsequently increases the photocurrent. In exp. 6, the inclusion of EVP results in a smaller positive photocurrent than in exp. 5, due to the accumulation of negative charge at the cathode from the reduction of EVP. Inclusion of

Table 2 Observed limiting photocurrent ($t = 100$ s) under visible light illumination with assembled electrodes[a]

Exp.	Photoanode	Cathode	j_{lim}/μA cm^{-2}
1	$TiO_2/F:SnO_2$	$TiO_2/F:SnO_2$	—[b]
2		$EVP/TiO_2/F:SnO_2$	—[b]
3		$Pt/TiO_2/F:SnO_2$	—[b]
4		$EVP/Pt/TiO_2/F:SnO_2$	—[b]
5	$RuL_2L'^{2+}/TiO_2/F:SnO_2$	$TiO_2/F:SnO_2$	0.006
6		$EVP/TiO_2/F:SnO_2$	0.003
7		$Pt/TiO_2/F:SnO_2$	0.010
8		$EVP/Pt/TiO_2/F:SnO_2$	0.008
9	$RuL_2L'^{2+}/RuO_2:TiO_2/F:SnO_2$	$TiO_2/F:SnO_2$	0.021
10		$EVP/TiO_2/F:SnO_2$	0.027
11		$Pt/TiO_2/F:SnO_2$	0.104
12		$EVP/Pt/TiO_2/F:SnO_2$	0.157

[a] Illumination with LED source. Incident power intensity = 3.81 mW cm^{-2}. [b] Measured photocurrents were below resolution of instrumentation.

Pt on the surface of the cathode in exp. 7 again improves the performance of the system due to the catalytic nature of Pt. In exp. 8, the inclusion of EVP as an electron shuttle does not have a substantial effect as electronic reduction decreases the photocurrent. The photocurrent measurements obtained in exp. 9–12 are an order of magnitude greater than those discussed in exp. 1–8 showing the importance of the anode catalyst RuO_2.

Fig. 1 depicts the transient photocurrent of exp. 9 compared with that obtained for exp. 1. The photocurrent yield of exp. 9 was significantly improved over that of exp. 1 with the profile resembling that of a PEC cell. The onset photocurrent on irradiation was sharp indicating charging of the electrical double layer followed by a quasi-steady-state current. This was expected since the oxidation species, water, was in relative excess and the system was therefore not concentration-diffusion limited. The photocurrent was observed to increase over time before reaching j_{lim} around 140 seconds.

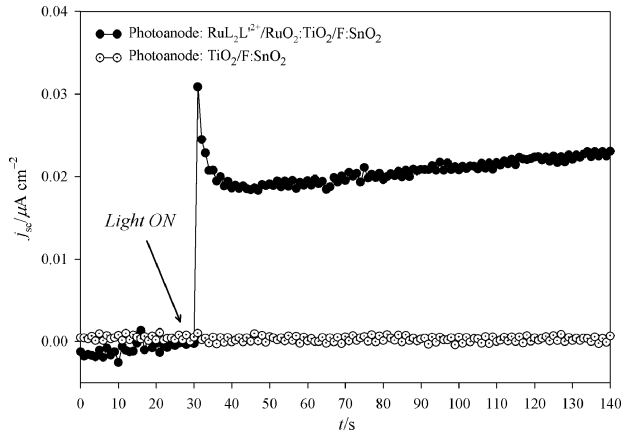

Fig. 1 Photocurrent observed for a TiO_2/F:SnO_2 cathode against the indicated photoanode irradiated with the white light LED source (3.81 mW cm^{-2}) in H_2O with Li_2SO_4 (0.5 M) as electrolyte (pH = 5.7).

The observed transient photocurrent of exp. 10 (Fig. 2) are consistent with that obtained for exp. 9. Although a larger peak photocurrent and increased j_{lim}, in comparison, was observed for exp.10. The assembly has been modified by the adsorption of EVP, which allows for charge build up at the surface, providing an alternative electrochemical route for the reduction of water. The increased peak photocurrent results from fast electronic reduction of the EVP species which relaxes into a steady-state electron transfer to water. Analogous to exp. 9, double layer charging was followed by quasi-steady-state oxidation.

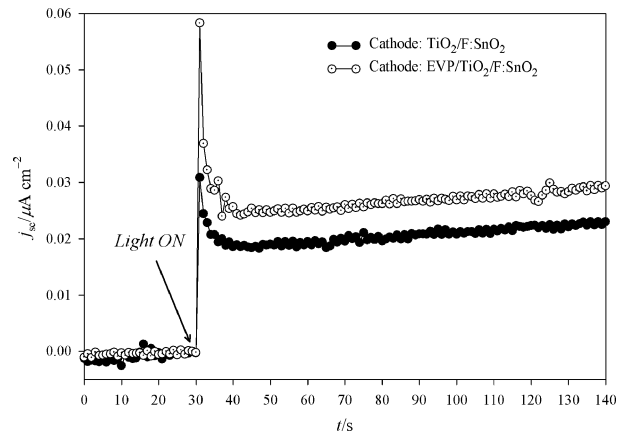

Fig. 2 Photocurrent observed for the $RuL_2L'^{2+}/RuO_2$:TiO_2/F:SnO_2 photoanode irradiated against the indicated cathodes. Experimental conditions are for those described in Fig. 1.

The transient photocurrent of exp. 11 and 9 are compared in Fig. 3. The photocurrent onset was intense upon illumination yet there was an apparent absence of charging of the double layer. The inclusion of Pt at the cathode increases the cathodic exchange current density, due to its catalytic nature, and is evident from the increased j_{lim}. The capacitive nature of the assembly was also clear from the gradual increase in j_{sc} from the initial irradiation until j_{lim} was reached.

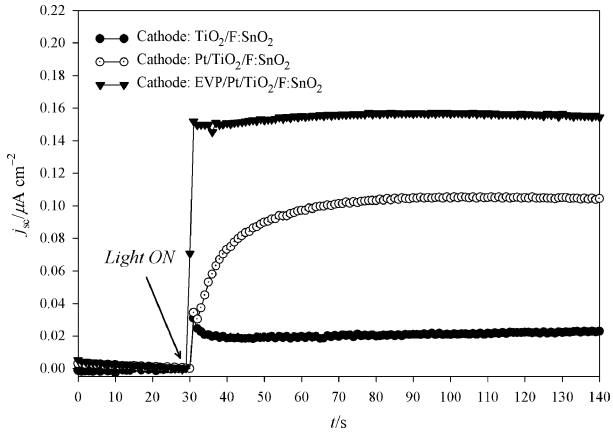

Fig. 3 Photocurrent observed for the $RuL_2L'^{2+}/RuO_2$:TiO_2/F:SnO_2 photoanode irradiated against the indicated cathodes. Experimental conditions are for those described in Fig. 1.

The transient photocurrent for exp. 12, compared to exp. 9 and 11, yields a large increase in j_{lim}, Fig. 3. Chemisorption of EVP to the platinised TiO_2 surface gives a favourable and well-defined change in the transient and steady state photocurrent. Observation of surface capacitance was eliminated and steady-state oxidation was apparent from initial illumination. An immediate steady-state process indicates that charging of the double layer and of the assembly components was negligible. This suggests that the process was under activation control with the elimination of the surface charging and build-up of electrons at the two electrodes within the resolution of these experiments.

Influence of pH on photocurrent yield

The effect of pH on the photochemical reaction is shown in Fig. 4. The yield, represented as the j_{lim} from the PCC, showed an optimum at pH 5. This value is consistent with earlier[15] estimations of similar particulate systems although it does conflict with that of Hirano *et al.*[38] For the systems presented in this paper surface protonation affects heterosupramolecular

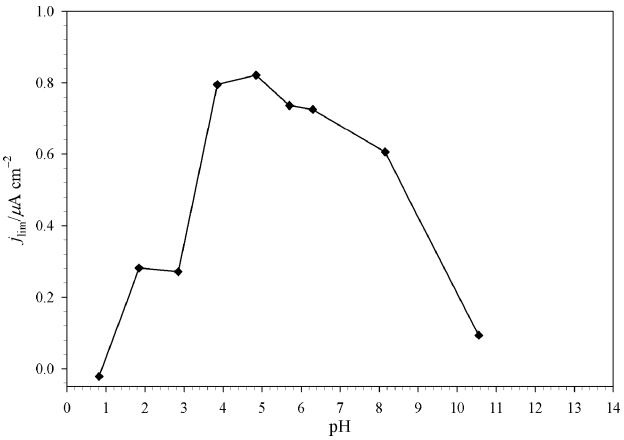

Fig. 4 Relationship of pH to the photochemical reaction. Adjustment to pH was with either HCl or NaOH. Cell assembly: $RuL_2L'^{2+}/RuO_2$:TiO_2/F:SnO_2|(0.5 M Li_2SO_4)|EVP/Pt/TiO_2/F:SnO_2; Xe lamp (12.0 mW cm^{-2}); AM 1.5 conditions, Oriel cut-off filter (# 66420).

assemblies according to the change in flatband potential, V_{FB} [eqn. (3)]:[39]

$$V_{FB} = -0.400–0.06\ \text{pH (V/SCE)} \quad (3)$$

For the PS, $E_{\frac{1}{2}}$ ($Ru^{III/II}$) = +1.26 V and E_{00} = 1.96 eV.[32] Thus at high pH V_{FB} exceeds the energy of the excited electron. Hence electron injection into the TiO_2 CB was unfavourable for pH > 5 (V_{FB} < −0.70 V). It is feasible that photons with energy exceeding the MLCT are able to inject, however maximum injection efficiency would occur at a pH ≤ 5. It would also be expected that at a pH lower than 5 the potential of the electrons being transferred to the cathode would be lower as these would assume the potential of the CB in the TiO_2. The lowering of the potential would thus reduce the driving force for reduction at the cathode and lower the overall current.

Coincidently, the pH of the studied solutions, as determined experimentally, provided conditions conductive to effective photochemical reaction.

Photoelectrochemical efficiency of optimised system

Fig. 5 presents the current density-voltage characteristics of the photochemical assembly of exp. 12 under AM 1.5 illumination from a Xe arc lamp and that of the LED source (Table 3).

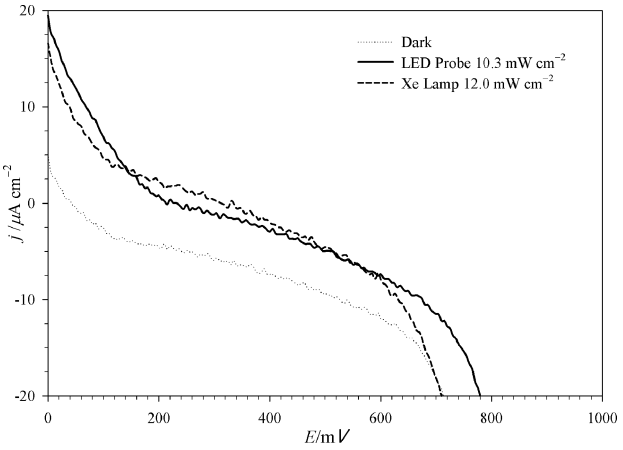

Fig. 5 Current density–voltage characteristics of photocatalytic cell at AM 1.5 illumination. Light intensities for light sources examined are as indicated. Active cell area: 0.16 cm^2.

The photocurrent density (j_{sc}), open-circuit photovoltage (V_{oc}) and fill factor (f) obtained under different illumination sources gives rise to considerable differences in power conversion efficiencies. The LED light source has a peak emission centred at 462 nm while the Xe lamp, simulating AM 1.5 conditions, has a broad photonic spectrum with a small percentage of overall light from the 455 nm region. The absorbed sensitiser has a broad MLCT at 455 nm, thus the system can be expected to respond favourably to the LED source and accordingly yield higher efficiencies.

The data illustrates that the device does not respond as a simple diode such as the DSC. When the applied potential across the cell was zero, j_{sc} was measured before a sudden change in the current as the applied potential scanned more positive. The drop in current in the light was due to the capacitive nature of the system prior to a positive current flow starting at ~200 mV. The current then further increases until V_{oc} was reached.

A comparative estimation of the photonic yield was obtained using the apparent quantum yield (AQY) in eqn. (4):[40]

$$\text{AQY}(\%) = \frac{\text{Number of reacted electrons } (j_{sc})}{\text{Number of absorbed incident photons}} \times 100 \quad (4)$$

The efficiency of the device for absorbed photons over the 420–700 nm range under steady-state conditions gives AQY = 1.6% (corrected against substrate attenuation) under AM 1.5 illumination. The calculated quantum yield was comparable to that reported by Tsuji *et al.*,[40] considering the variation in the experimental conditions between the two systems.

The photoelectrochemical system

The data presented demonstrates that the measurement of j_{sc} was possible in an aqueous electrolyte under visible light irradiation with no applied potential. The basis of this system can be described as a series of functioning units: (i) light absorption by a PS; (ii) electron injection; (iii) electron transport *via* a semiconducting substrate; (iv) electronic reduction of an electron shuttle; and (v) subsequent reduction at the cathode. The linking of each of the individual components, and their intrinsic properties, required for the function of H_2O photolysis constitutes a heterosupramolecular assembly. Hence, the purpose of each component in the assembly can be described and rationalised in terms of its own intrinsic function. While we have not attempted to detect either O_2 or H_2 from water photolysis we have, in accordance with most other work in the field, accepted this as the most likely photoelectrochemical reaction occuring in the cell, and explicitly base our discussion on this assumption. When a photon of light with sufficient energy to induce charge separation was incident with the adsorbed PS, excitation, ionisation and subsequent oxidation of the PS occurs according to eqn. (5).

$$TiO_2–RuL_2L'^{2+} + h\nu \rightarrow e^-_{(cb)} + TiO_2–RuL_2L'^{3+} \quad (5)$$

With the injected electron partitioned in the CB of TiO_2 charge recombination was prevented and the PS^+ was available as a reactive species. Laser flash photolysis experiments have shown that an oxidised PS, was capable of direct oxidation of water to O_2.[41] This was illustrated by the photocurrents observed in exp. 5–8. The irreversible photo-oxidation of PS preceding this step was a plausible source of the observed photocurrent. However, in Figs. 1–4 the photocurrent was observed to *increase* with time as opposed to a decrease if the surface concentration of PS^+ was to diminish.[42]

Further to these photocurrent observations, the excited state MLCT of tris-2,2′-bipyridine ruthenium(II) complexes (*e.g.* $RuL_2L'^{2+}$) has been described as $[Ru^{III}(bpy^{\bullet -})(bpy)_2]^{2+}$. That is, the ejected electron resides on only one of the three bpy ligands.[41,43] Comparative measurements of injection quantum yields on PSs with substituted bipyridine ligands have shown that $RuL_2L'^{2+}$, has $\phi = 0.5 \pm 0.1$. The yield of less than unity, $\phi < 1$, has been attributed to increased π^* energies of the surface bound ligand.[32] This would certainly be a contributing factor to the small photocurrent and efficiencies obtained in this study.

The inclusion of RuO_2 to the photochemical assembly significantly improved the cell performance. Increased photocurrents

Table 3 Photovoltaic parameters of PCC under different light sources[a]

Light source	P_{in}/mW cm^{-2}	j_{sc}/mA cm^{-2}	V_{oc}/mV	P_{max}/mW cm^{-2}	f	η(%)
LED source	10.3	19.5	735	0.736	0.0515	0.0072
Xe lamp	12.0	15.5	695	0.435	0.0415	0.0036

[a] Incident power intensity P_{in}; short-circuit photocurrent density: j_{sc}; open-circuit photovoltage: V_{oc}; maximum electricity output power density: P_{max}; fill factor: $f = P_{max}/P_{in}$; conversion efficiency: $\eta = (P_{max} \times f/P_{in}) \times 100\%$; Active cell area: 0.16 cm^2.

in exp. 9–12 due to the specific catalytic function of the metal-oxide occur according to eqn. (6):

$$RuO_{2(bulk)} + H_2O_{(aq)} \rightarrow \frac{1}{2}O_{2(ads)} + 2H^+_{(aq)} + e^-_{(ads)} \quad (6)$$

RuO_2 behaves as an electron hole trap following photo-oxidation of $RuL_2L'^{2+}$ in eqn. (5). Although PS^+ was capable of direct oxidation of H_2O, eqn. (6) and subsequently (7) are favoured. The larger (~30 nm) RuO_2 particle acts as an electron donor to regenerate the PS.[17,44]

$$TiO_2–RuL_2L'^{3+} + e^-_{(ads)} \rightarrow TiO_2–RuL_2L'^{2+} \quad (7)$$

The preference of the system for eqn. (6) was evident in the capacitive component present in the system. Sufficient negative charge accumulates on the surface of RuO_2 before partial discharge occurs according to eqn. (8):

$$2 \times \frac{1}{2}O_{2(abs)} \rightarrow O_{2(abs)} \rightarrow O_{2(aq)} \quad (8)$$

However, a limitation of RuO_2 in the system was its capability of catalysing the reversible reaction, eqn. (9):[44]

$$2OH^-_{(ads)} \rightleftarrows O_{2(aq)} + 2H^+_{(aq)} + 4e^- \quad (9)$$

Therefore, in the presence of an oxygenated solution the reverse reaction would suppress oxidation and limit photolysis. This competitive reaction, occurring at the surface of the anode, would act as a short circuit in the cell and reduce the overall photocurrent yield.

The response of EVP modified electrodes V and VI illustrate that the electron shuttle, EVP, affords an active function in the reduction process. This was facilitated by the presence of a Pt catalyst. Electrons in the CB traverse the external circuit to EVP on the surface, reducing the electron shuttle molecule according to eqn. (10):

$$e^-_{(cb)} + TiO_2–EVP^{2+} \rightarrow TiO_2–EVP^+ \quad (10)$$

Direct electron accumulation from the CB of TiO_2 at surface bound Pt [eqn. (11)] was supported by the transients in Fig. 3.

$$e^-_{(cb)} \rightarrow e^-_{(Pt)} \quad (11)$$

However, the enhanced photocurrents of Fig. 3 (exp. 12) indicate that the presence of EVP provides a more energetically favourable route for the migration of electrons to the surface Pt [eqn. (12)]. Thus, EVP functions effectively in the system as an electron shuttle contributing to the photochemical assembly.

$$TiO_2–EVP^+ \rightarrow e^-_{(Pt)} + TiO_2–EVP^{2+} \quad (12)$$

Increase in the photocurrent yield for experiments involving electrodes V and VI can be rationalised by the presence of Pt.[45] The ballistic transfer of electrons to-and-over the Schottky barrier enhance photocurrent yields. Electrons in the CB and those relayed by EVP accumulate on the surface of Pt and react according to eqn. (13–15):[46,47]

$$H^+_{(aq)} \rightarrow H^+_{(Pt)} \quad (13)$$

$$H^+_{(Pt)} + e^-_{(aq)} \rightarrow H^{\bullet}_{(Pt)} \quad (14)$$

$$2H^{\bullet}_{(Pt)} \rightarrow H_{2(Pt)} \rightarrow H_{2(aq)} \quad (15)$$

The diffusion and then migration of hydrogen ions [eqn. (13)] to the surface of Pt precedes their reduction to the hydrogen radical [eqn. (14)]. The ease of the reactions described by eqn. (14) and (15) and the decreased overpotential affords H_2 generation over platinised surfaces.[46] This enables atomic nucleation and subsequent ejection of diatomic H_2 from the surface.

Effectively a single electron ejected from the photo-ionisation of $RuL_2L'^{2+}$ affords the oxidation of H_2O by RuO_2 and regeneration of $RuL_2L'^{2+}$. The ejected electron, if sufficient in energy, was all that was required to reduce EVP, accumulate charge on Pt and subsequently reduce H_2O.

Conclusion

The report presented summarises the study of a multi-component photochemical system involving molecular and condensed phase components with specific functions. It has been demonstrated that a heterosupramolecular assembly is capable of inducing a photochemical reaction, in water, under visible irradiation with the process identified and monitored by the measurement of a short circuit current. This process has not been identified previously by the instrumental methods implemented in this work.

$$RuL_2L'^{2+}/RuO_2{:}TiO_2/F{:}SnO_2|(0.5\ M\ Li_2SO_4)|EVP/Pt/TiO_2/F{:}SnO_2$$

was found to be the most efficient cell assembly. The optimised conditions of the electrolyte solution were determined to be pH = 5 where under illumination from the Xe light source, the assembly yielded $\eta = 0.0036\%$ with an apparent quantum yield (AQY) of 1.6%.

Acknowledgements

Financial support of this work by the former Centre of Instrumental and Developmental Chemistry, Inorganic Materials Research Program, and the Queensland Government Smart State Initiative, is gratefully acknowledged. The authors would like to thank George Racz for technical support in configuring equipment.

References

1 U. Diebold, The surface science of titanium dioxide, *Surf. Sci. Rep.*, 2003, **48**, 53–229.
2 A. L. Linsebigler, G. Lu and J. T. Yates, Jr., Photocatalysis on TiO_2 surfaces: Principles, mechanisms, and selected results, *Chem. Rev.*, 1995, **95**, 735–758.
3 A. Fujishima and K. Honda, Electrochemical photolysis of water at a semiconductor electrode, *Nature*, 1972, **238**, 37–38.
4 T. Sreethawong, Y. Suzuki and S. Yoshikawa, Photocatalytic evolution of hydrogen over nanocrystalline mesoporous titania prepared by surfactant-assisted templating sol-gel process, *Catal. Commun.*, 2005, **6**, 119–124.
5 Q.-L. Zhang, L.-C. Du, Y.-X. Weng, L. Wang, H.-Y. Chen and J.-Q. Li, Particle-size-dependent distribution of carboxylate adsorption sites on TiO_2 nanoparticle surfaces: Insights into the surface modification of nanostructured TiO_2 electrodes, *J. Phys. Chem. B*, 2004, **108**, 15077–15083.
6 T.-V. Nguyen, S. Kim and O.-B. Yang, Water decomposition on TiO_2–SiO_2 and RuS_2/TiO_2–SiO_2 photocatalysts: The effect of electronic characteristics, *Catal. Commun.*, 2004, **5**, 59–62.
7 N. Serpone, J. Martin, S. Horikoshi and H. Hidaka, Photocatalyzed oxidation and mineralization of C1–C5 linear aliphatic acids in UV-irradiated aqueous titania dispersions-kinetics, identification of intermediates and quantum yields, *J. Photochem. Photobiol., A*, 2005, **169**, 235–251.
8 T. Tachikawa, S. Tojo, M. Fujitsuka and T. Majima, Photocatalytic one-electron oxidation of biphenyl derivatives strongly coupled with the TiO_2 surface, *Langmuir*, 2004, **20**, 2753–2759.
9 D. L. Jiang, H. J. Zhao, S. Q. Zhang and R. John, Kinetic study of photocatalytic oxidation of adsorbed carboxylic acids at TiO_2 porous films by photoelectrolysis, *J. Catal.*, 2004, **223**, 212–220.
10 A. Topalov, D. Molnar-Gabor, B. Abramovic, S. Korom and D. Pericin, Photocatalytic removal of the insecticide fenitrothion from water sensitized with TiO_2, *J. Photochem. Photobiol., A*, 2003, **160**, 195–201.
11 M. Suzuki, C. C. Waraksa, T. E. Mallouk, H. Nakayama and K. Hanabusa, Enhanced photocatalytic reduction of methyl viologen by self-assembling ruthenium(II)poly(pyridyl) complexes with l-lysine containing side chains, *J. Phys. Chem. B*, 2002, **106**, 4227–4231.
12 M. Sakamoto, T. Kamachi, I. Okura, A. Ueno and H. Mihara, Photoinduced hydrogen evolution with peptide dendrimer-multi-Zn(II)-porphyrin, viologen, and hydrogenase, *Biopolymers*, 2001, **59**, 103–109.

13 N. Asakura, T. Hiraishi, T. Kamachi and I. Okura, Photoinduced hydrogen evolution with cytochrome c_3-viologen-ruthenium(II) triad complex and hydrogenase, *J. Mol. Catal. A: Chem.*, 2001, **172**, 1–7.

14 E. Amouyal, Photochemical production of hydrogen and oxygen from water - a review and state of the art, *Sol. Energy Mater. Sol. Cells*, 1995, **38**, 249–276.

15 A. Moradpour, E. Amouyal, P. Keller and H. Kagan, Hydrogen production by visible light irradiation of aqueous solutions of tris(2,2′-bipyridine)ruthenium(2+), *Nouv. J. Chim.*, 1978, **2**, 547–549.

16 K. Kalyanasundaram, J. Kiwi and M. Grätzel, Hydrogen evolution from water by visible light, a homogeneous three component test system for redox catalysis, *Helv. Chim. Acta*, 1978, **61**, 2720–2730.

17 K. Kalyanasundaram and M. Grätzel, Cyclic cleavage of water into H_2 and O_2 by visible light with coupled redox catalysts, *Angew. Chem., Int. Ed. Engl.*, 1979, **18**, 701–702.

18 D. Duonghong, E. Borgarello and M. Grätzel, Dynamics of light-induced water cleavage in colloidal systems, *J. Am. Chem. Soc.*, 1981, **103**, 4685–4690.

19 D. Duonghong, N. Serpone and M. Grätzel, Integrated systems for water cleavage by visible light; sensitization of titanium dioxide particles by surface derivatization with ruthenium complexes, *Sci. Pap. Inst. Phys. Chem. Res. (Jpn.)*, 1984, **78**, 232–236.

20 A. Harriman, The photogeneration of hydrogen, *Platinum Met. Rev.*, 1991, **35**, 22–23.

21 P. Keller, A. Moradpour, E. Amouyal and H. B. Kagan, Hydrogen production by visible-light using viologen-dye mediated redox cycles, *Nouv. J. Chim.*, 1980, **4**, 377–384.

22 J. Sato, H. Kobayashi, K. Ikarashi, N. Saito, H. Nishiyama and Y. Inoue, Photocatalytic activity for water decomposition of RuO_2-dispersed Zn_2GeO_4 with d^{10} configuration, *J. Phys. Chem. B*, 2004, **108**, 4369–4375.

23 K. Ikarashi, J. Sato, H. Kobayashi, N. Saito, H. Nishiyama and Y. Inoue, Photocatalysis for water decomposition by RuO_2-dispersed $ZnGa_2O_4$ with d^{10} configuration, *J. Phys. Chem. B*, 2002, **106**, 9048–9053.

24 S. Licht, B. Wang, S. Mukerji, T. Soga, M. Umeno and H. Tributsch, Efficient solar water splitting, exemplified by RuO_2-catalyzed AlGaAs/Si photoelectrolysis, *J. Phys. Chem. B*, 2000, **104**, 8920–8924.

25 J. M. Kleijn and G. K. Boschloo, The influence of the preparation temperature of colloidal ruthenium dioxide on the photosensitized reduction of hydrogen ions, *J. Electroanal. Chem. Interfacial Electrochem.*, 1991, **300**, 595–606.

26 J. M. Kleijn and J. Lyklema, Colloid-chemical properties of ruthenium dioxide in relation to catalysis of the photochemical generation of hydrogen, *Colloid Polym. Sci.*, 1987, **265**, 1105–1113.

27 P. Keller, A. Moradpour and E. Amouyal, Ruthenium dioxide: A redox catalyst for the generation of hydrogen from water, *J. Chem. Soc., Faraday Trans. 1*, 1982, **78**, 3331–3340.

28 A. Currao, V. Raja Reddy, M. K. van Veen, R. E. I. Schropp and G. Calzaferri, Water splitting with silver chloride photoanodes and amorphous silicon solar cells, *Photochem. Photobiol. Sci.*, 2004, **3**, 1017–1025.

29 X. Marguerettaz and D. Fitzmaurice, Heterosupramolecular chemistry: Long-lived charge trapping by vectorial electron flow in a heterotriad, *J. Am. Chem. Soc.*, 1994, **116**, 5017–5018.

30 X. Marguerettaz, R. O'Neill and D. Fitzmaurice, Heterodyads: Electron transfer at a semiconductor electrode-liquid electrolyte interface modified by an adsorbed spacer-acceptor complex, *J. Am. Chem. Soc.*, 1994, **116**, 2629–2630.

31 G. J. Wilson and G. Will, Photocleavage of water with a photochemical heterosupramolecular assembly, *Curr. Appl. Phys.*, 2004, **4**, 351–354.

32 I. Gillaizeau-Gauthier, F. Odobel, M. Alebbi, R. Argazzi, E. Costa, C. A. Bignozzi, P. Qu and G. J. Meyer, Phosphonate-based bipyridine dyes for stable photovoltaic devices, *Inorg. Chem.*, 2001, **40**, 6073–6079.

33 B. P. Sullivan, D. J. Salmon and T. J. Meyer, Mixed phosphine 2,2′-bipyridine complexes of ruthenium, *Inorg. Chem.*, 1978, **17**, 3334–3341.

34 S. Ardizzone, P. Siviglia and S. Trasatti, The point of zero charge of ruthenium dioxide, *J. Electroanal. Chem. Interfacial Electrochem.*, 1981, **122**, 395–401.

35 B. O'Regan, J. Moser, M. Anderson and M. Grätzel, Vectorial electron injection into transparent semiconductor membranes and electric field effects on the dynamics of light-induced charge separation, *J. Phys. Chem.*, 1990, **94**, 8720–8726.

36 G. Will, G. Boschloo, R. Hoyle, S. N. Rao and D. Fitzmaurice, Potentiostatic modulation of the direction of light-induced electron transfer in a heterosupermolecule, *J. Phys. Chem. B*, 1998, **102**, 10272–10278.

37 R. Cinnsealach, G. Boschloo, S. Nagaraja Rao and D. Fitzmaurice, Colored electrochromic windows based on nanostructured TiO_2 films modified by adsorbed redox chromophores, *Sol. Energy Mater. Sol. Cells*, 1999, **57**, 107–125.

38 K. Hirano, E. Suzuki, A. Ishikawa, T. Moroi, H. Shiroishi and M. Kaneko, Sensitization of TiO_2 particles by dyes to achieve H_2 evolution by visible light, *J. Photochem. Photobiol., A*, 2000, **136**, 157–161.

39 G. Rothenberger, D. Fitzmaurice and M. Grätzel, Spectroscopy of conduction band electrons in transparent metal oxide semiconductor films: Optical determination of the flatband potential of colloidal titanium dioxide films, *J. Phys. Chem.*, 1992, **96**, 5983–5986.

40 I. Tsuji, H. Kato, H. Kobayashi and A. Kudo, Photocatalytic η_2 evolution reaction from aqueous solutions over band structure-controlled $(AgIn)_xZn_{2(1-x)}S_2$ solid solution photocatalysts with visible-light response and their surface nanostructures, *J. Am. Chem. Soc.*, 2004, **126**, 13406–13413.

41 M. Goez, D. Von Ramin-Marro, M. H. O. Musa and M. Schiewek, Photoionization of $[Ru(bpy)_3]^{2+}$: A catalytic cycle with water as sacrificial donor, *J. Phys. Chem. A*, 2004, **108**, 1090–1100.

42 J. A. Treadway, J. A. Moss and T. J. Meyer, Visible region photooxidation on TiO_2 with a chromophore-catalyst molecular assembly, *Inorg. Chem.*, 1999, **38**, 4386–4387.

43 P. S. Braterman, A. Harriman, G. A. Heath and L. J. Yellowlees, The electronic absorption spectrum and structure of the emitting state of the tris(2,2′-bipyridyl)ruthenium(II) complex ion, *J. Chem. Soc., Dalton Trans.*, 1983, 1801–1803.

44 N. Serpone, E. Pelizzetti and M. Grätzel, Photosensitization of semiconductors with transition metal complexes—a route to the photoassisted cleavage of water, *Coord. Chem. Rev.*, 1985, **64**, 225–245.

45 E. W. McFarland and J. Tang, A photovoltaic device structure based on internal electron emission, *Nature*, 2003, **421**, 616–618.

46 R. Fretwell and P. Douglas, Nanocrystalline-TiO_2-Pt photo-electrochemical cells-UV induced hydrogen evolution from aqueous solutions of alcohols, *Photochem. Photobiol. Sci.*, 2002, **1**, 793–798.

47 P. Pichat, M. N. Mozzanega, J. Disdier and J. M. Herrmann, Platinum content and temperature effects on the photocatalytic hydrogen production from aliphatic alcohols over platinum/titanium dioxide, *Nouv. J. Chim.*, 1982, **6**, 559–564.